iScience

CellPress
OPEN ACCESS

Article

An efficient Pt@MXene platform for the analysis of small-molecule natural products

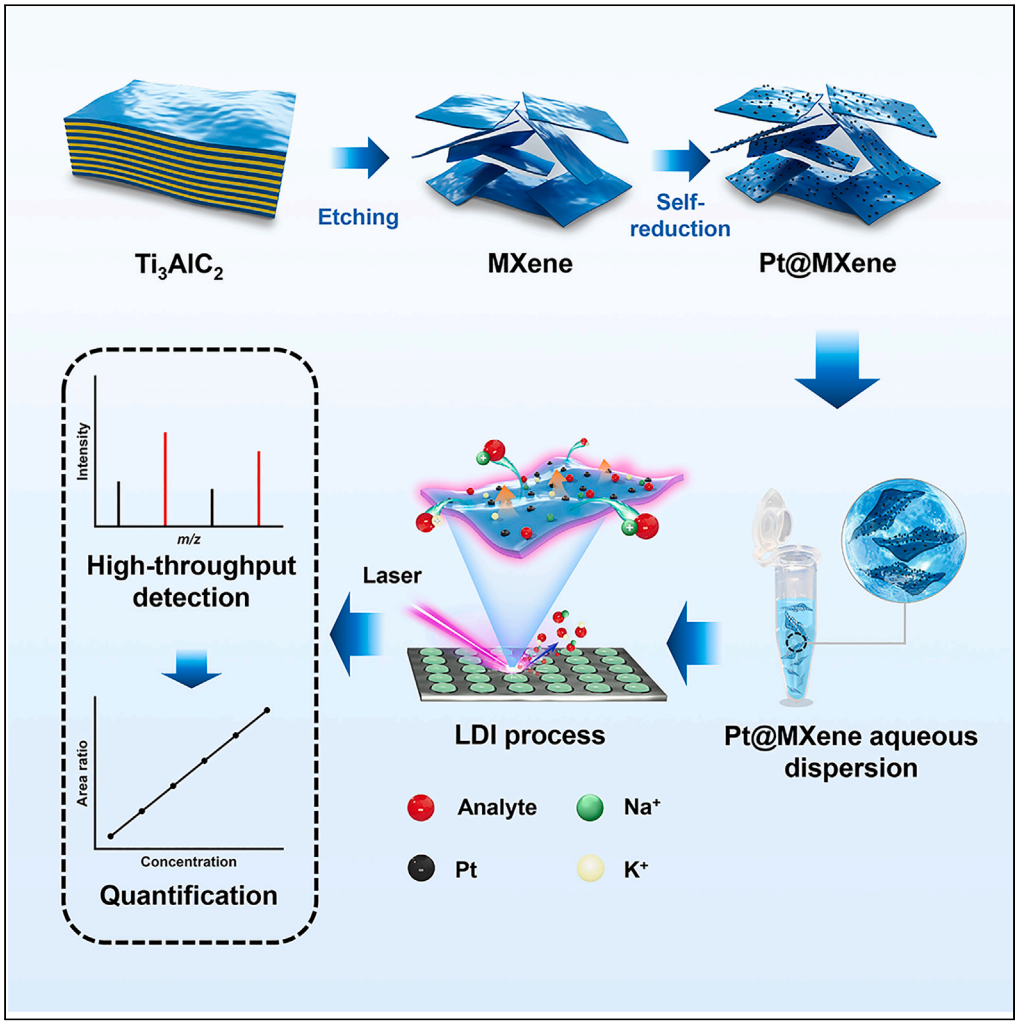

Guanhua Zhang, Chunxia Ma, Qing He, ..., Lingyu Li, Yan Wang, Xiao Wang

machunxia8927@163.com (C.M.)
wangx@sdas.org (X.W.)

Highlights

An ideal Pt@MXene nanosubstrate was synthesized for SALDI MS analysis

Pt@MXene platform is suitable for the analysis of various small-molecule natural products

Pt@MXene platform enables high-throughput detection in complex biosamples

Pt@MXene platform can accurately quantify small-molecule natural products

Zhang et al., iScience 26, 106622
May 19, 2023
https://doi.org/10.1016/j.isci.2023.106622

iScience

CellPress
OPEN ACCESS

Article

An efficient Pt@MXene platform for the analysis of small-molecule natural products

Guanhua Zhang,[1,2] Chunxia Ma,[2,5,*] Qing He,[3] Hongjing Dong,[2] Li Cui,[2] Lili Li,[2] Lingyu Li,[4] Yan Wang,[1] and Xiao Wang[1,2,*]

SUMMARY

Small-molecule (*m/z*<500) natural products have rich biological activity and significant application value thus need to be effectively detected. Surface-assisted laser desorption/ionization mass spectrometry (SALDI MS) has become a powerful detection tool for small-molecule analysis. However, more efficient substrates need to be developed to improve the efficiency of SALDI MS. Thus, platinum nanoparticle-decorated Ti_3C_2 MXene (Pt@MXene) was synthesized in this study as an ideal substrate for SALDI MS in positive ion mode and exhibited excellent performance for the high-throughput detection of small molecules. Compared with using MXene, GO, and CHCA matrix, a stronger signal peak intensity and wider molecular coverage was obtained using Pt@MXene in the detection of small-molecule natural products, with a lower background, excellent salt and protein tolerance, good repeatability, and high detection sensitivity. The Pt@MXene substrate was also successfully used to quantify target molecules in medicinal plants. The proposed method has potentially wide application.

INTRODUCTION

Small-molecule (*m/z*<500) natural products in plants, including amino acids, carbohydrates, phytohormones, organic acids, and alkaloids, perform several important functions for the viability of organisms.[1] These products also exhibit rich physiological and pharmacological activities and are widely used in the fields of medicine, chemistry, and food.[2] The metabolic pathways, varieties, and physiological characteristics of different plants may lead to differences in the species and content levels of small-molecule natural products.[3,4] Consequently, comprehensive, accurate, and reliable detection of small-molecule natural products is imperative and can contribute to metabolomic research, species identification, and elucidation of the growth mechanism of plants. Currently, the analysis of small-molecule natural products is typically performed using thin-layer chromatography (TLC), high-performance liquid chromatography (HPLC), and liquid chromatography–mass spectrometry (LC–MS). These methods usually have good analytical capabilities. However, these methods also have significant shortcomings, including complex sample preparation, low throughput, the need for additional derivatization procedures, and large solvent consumption, and can therefore be slow, laborious, and expensive.[5–7] Hence, a rapid and comprehensive small-molecule natural product analysis technology is urgently needed.

Surface-assisted laser desorption/ionization (SALDI) mass spectrometry (MS) has emerged in the past decade as a powerful technology for the detection of small-molecule natural products.[8] In SALDI MS, an optical-thermal conversion process enables energy transfer from the substrate to the analyte deposited on its surface, facilitating desorption/ionization of analyte molecules.[9] Similar to classical matrix-assisted laser desorption/ionization (MALDI) MS, SALDI MS only requires replacing the traditional organic matrices into nanomaterials or structured inorganics as substrates. Generally, inorganic substrates of SALDI MS can exhibit superior UV laser absorption, better efficiency energy transfer and higher physical/chemical stability than conventional matrices.[10] The samples exhibited various desorption/ionization efficiency because of differences in the substrates. Some materials with surface modification have been also employed to select the adsorption of small molecules in LDI MS analysis.[11] Therefore, SALDI MS eliminates some limitations of MALDI MS. Examples of these limitations are that organic matrices, such as 2,5-dihydroxybenzoic acid (DHB) and α-cyano-4-hydroxycinnamic acid (CHCA), undergo non-uniform co-crystallization with a sample, resulting in poor repeatability, and the matrix background interferes with the detection of small-molecule natural products.[12] In some cases, organic matrix effects can hinder the ionization of small-molecule

[1]College of Traditional Chinese Medicine, Yunnan University of Chinese Medicine, Kunming, Yunnan 650500, China

[2]Key Laboratory for Applied Technology of Sophisticated Analytical Instruments of Shandong Province, Shandong Analysis and Test Center, Qilu University of Technology (Shandong Academy of Sciences), Jinan, Shandong 250014, China

[3]Collaborative Innovation Center of Steel Technology, University of Science and Technology Beijing, Beijing 100083, China

[4]Key Laboratory of Food Processing Technology and Quality Control of Shandong Higher Education Institutes, College of Food Science and Engineering, Shandong Agricultural University, Taian, Shandong 271018, China

[5]Lead contact

*Correspondence: machunxia8927@163.com (C.M.), wangx@sdas.org (X.W.)

https://doi.org/10.1016/j.isci.2023.106622

analytes.[13,14] In addition, SALDI MS can enhanced detection sensitivity by tens of times compared to conventional MALDI MS,[15] allowing microanalysis (~pmol, ~fmol) for natural products in bio-samples.[16] Thus, a large number of nanomaterial substrates have been developed for laser desorption/ionization (LDI) MS, such as graphene,[17] TiO_2 nanoparticles (NPs),[18] metal NPs,[19] and MXenes.[20] Among these substrates, MXenes are emerging two-dimensional nanomaterials with excellent hydrophilicity, high ultraviolet–visible (UV–Vis) absorption, good charge mobility,[21] and extensive application prospects for SALDI MS.

The chemical formula of MXenes is $M_{n+1}X_nT_x$ (n = 1–3). M, X, and T represent transition metals (such as Ti, V, and Mo), C and/or N, and surface termination groups (such as-O,-F, and-OH), respectively.[22] Ti_3C_2 MXene (denoted as MXene) is a representative MXenes that has received extensive attention. Abundant functional groups on the MXene surface can promote the adsorption of small-molecule natural products and the enrichment and transference of Na^+ or K^+. Previous studies have shown that MXene can facilitate more effective SALDI MS detection than graphene oxide (GO), carbon nanotubes (CNTs), and organic matrices (DHB and CHCA).[20,23] More importantly, MXene has a high surface area and surface defects/vacancies and can be used to support other heterogeneous materials to enhance SALDI MS performance.[24]

Precious-metal (Ag, Au, Pt) NPs have unique localized surface plasma resonance characteristics and outstanding optical-thermal conversion efficiency and are considered to be one of the most attractive nanomaterials for SALDI MS substrates.[25] However, Au or Ag NPs produce cluster ions that may interfere with detection in SALDI MS.[19,26] Pt NPs are a stable substrate that exhibits a clean background and high desorption/ionization efficiency in SALDI MS.[27,28] Pt NPs-decorated MXene (Pt@MXene) exhibits superior electrical conductivity and optical-thermal conversion properties than MXene.[29] In addition, Pt@MXene has highly biosafety both *in vitro* and *in vivo*, ensuring that no adverse effects are caused during use.[30,31] As a result of these good properties, Pt@MXene platforms have been mainly used in nanocatalysts, electrochemistry, and biomedicine.[30,32,33] However, the performance of Pt@MXene as a substrate for SALDI MS has not been determined to date.

Herein, Pt@MXene was synthesized by a simple and green approach (Scheme 1A), followed performed high-throughput detection and quantification of small-molecule natural products in two plant samples (Scheme 1B). Notably, the reaction is generated by self-reduction without the addition of a catalyst, enabling significant preservation of the original characteristics of MXene nanosheets. The efficacy of Pt@MXene has been demonstrated for the analysis of various small-molecule natural products. Pt@MXene has been found to have stronger UV–Vis absorption than MXene and can effectively absorb laser energy. Compared with the commonly used substrates (GO), MXene, and the organic matrix (CHCA), Pt@MXene exhibits superior performance for the detection of small-molecule natural products (amino acids, phytohormones, organic acids, alkaloids, and carbohydrates) in terms of a lower background interference, high sensitivity, good salt and protein tolerance, and reliable stability. Pt@MXene has also been used to successfully quantify small-molecule natural products of medicinal plants, including gentiopicroside (GP) in *Gentiana scabra* Bge. (*G. scabra*) and tanshinone IIA (TS) in *Salvia miltiorrhiza* Bge. (*S. miltiorrhiza*). A multifunctional detection platform for the high-throughput qualitative and quantitative analysis of small-molecule natural products in complex plant samples has been developed in this study.

RESULTS AND DISCUSSION

Preparation and characterization of Pt@MXene

The synthesis approach of Pt@MXene as depicted in Scheme 1A. Single/few-layer MXene nanosheets were prepared by etching Ti_3AlC_2 based on LiF/HCl method, followed by ultrasonication. The Pt@MXene nanocomposite was constructed by a top-down synthesis method (a self-reduction reaction) using single/few-layer MXene nanosheets and $H_2PtCl_6 \cdot 6H_2O$ as raw materials. Compared to other top-down synthetic methods (such as electrochemical exfoliation[34]) and bottom-up methods (such as atomic layer deposition[35] and electrodeposition[36]), the top-down synthesis method (a self-reduction reaction) applied in this study has the advantages of simpler, greener, and lower cost. More importantly, the interference of mass spectrometry analysis produced by reducing agent residue could also be avoided by using this top-down synthesis method (a self-reduction reaction) because no reducing agent was applied to the entire operation.

The transmission electron microscopy (TEM) image in Figure 1A shows the micromorphology of the MXene consisting of a monolayer or few layers of MXene nanosheets. The reaction produced Pt NPs dispersed on the surface of MXene nanosheets with an average particle size of approximately 2.56 nm (Figure 1B). The

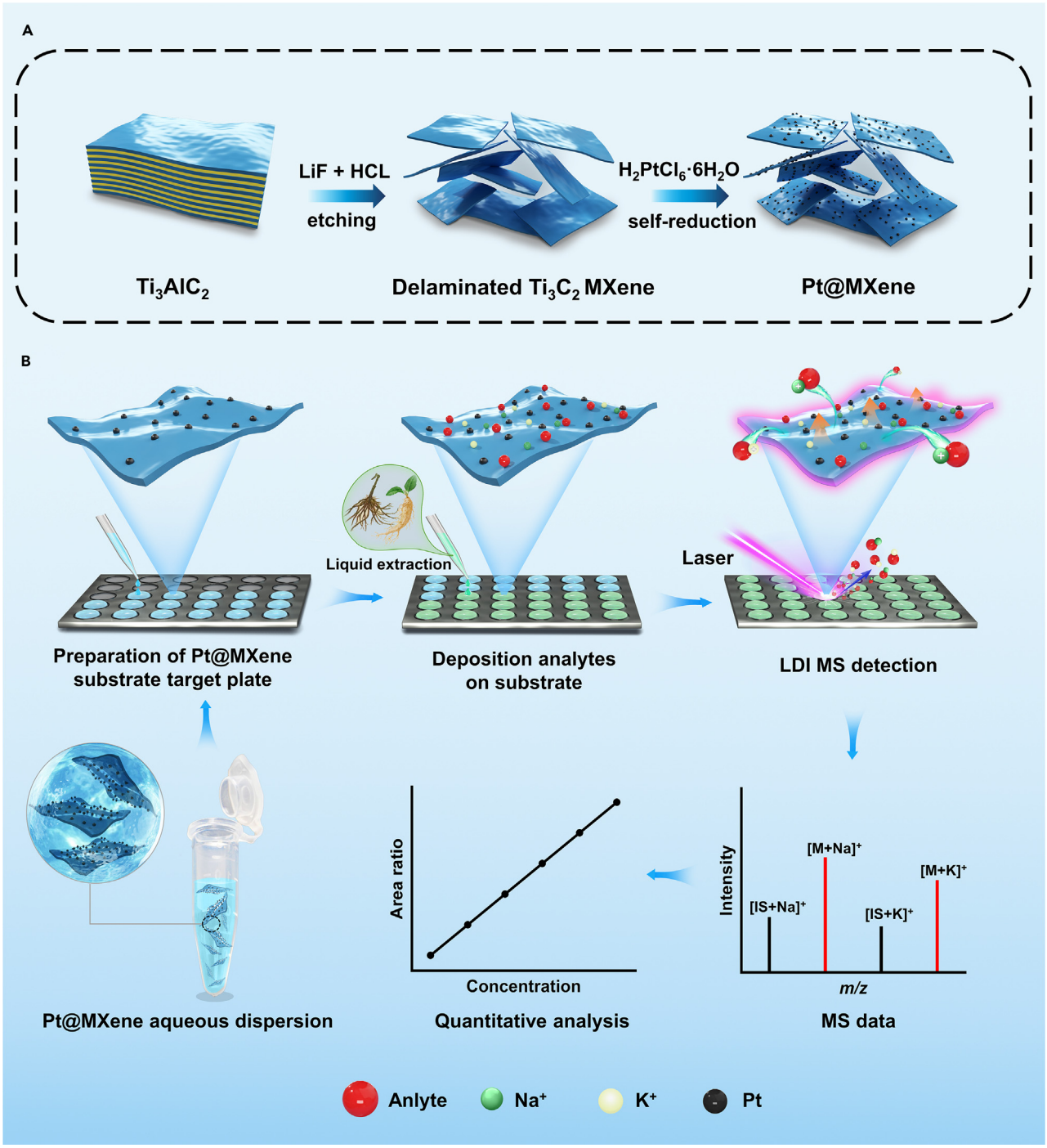

Scheme 1. Fabrication of Pt@MXene and a schematized workflow for the use of Pt@MXene as an ideal substrate for SALDI MS

(A) Synthesis process of the Pt@MXene nanocomposite.

(B) Schematized workflow for direct high-throughput detection and quantitative analysis of small-molecule natural products in plant samples by SALDI MS using Pt@MXene.

high-resolution TEM (HRTEM) image of Pt@MXene exhibited a 0.23-nm lattice fringe of Pt, assigned to the (111) plane (Figure 1C),[35] which proved the successful doping of Pt NPs into MXene. The types and distribution of elements in Pt@MXene are shown in the energy-dispersive X-ray spectroscopy (EDS) mapping spectrum. Figure 1D shows that Pt NPs were dispersed homogeneously on the surface of MXene, which

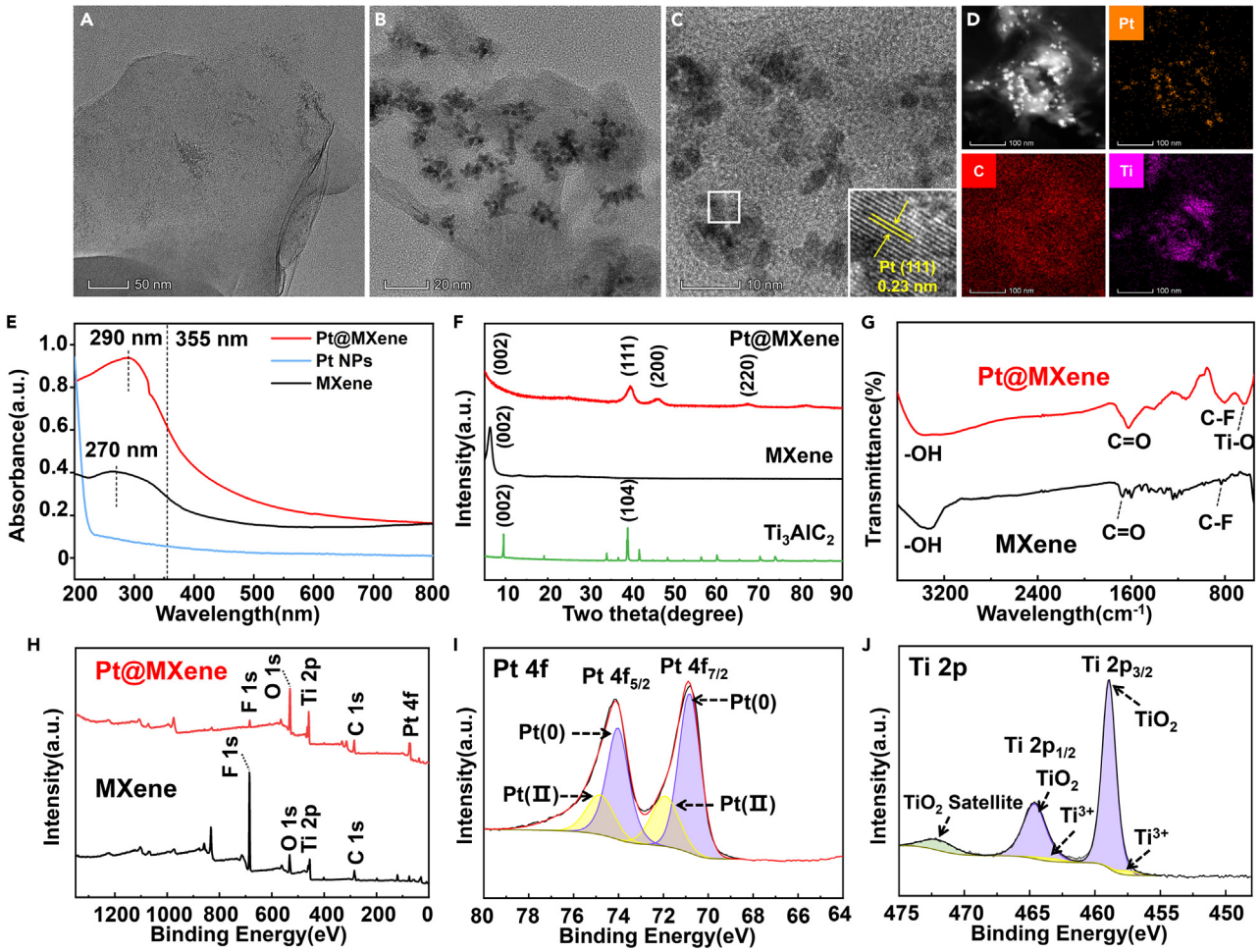

Figure 1. Construction and characterization of material

(A) TEM image of MXene.

(B) TEM image of Pt@MXene.

(C and D) HAADF-STEM and corresponding elemental mapping images of Pt@MXene.

(E) UV–Vis spectra of Pt@MXene, Pt NPs, and MXene.

(F) XRD patterns of Pt@MXene, MXene, and Ti_3AlC_2.

(G) FT-IR spectrum of Pt@MXene and MXene.

(H) Survey XPS spectrum of Pt@MXene and MXene.

(I) High-resolution XPS spectra of Pt 4f in Pt@MXene.

(J) High-resolution XPS spectra of Ti 2p in Pt@MXene.

was consistent with the HRTEM detection result. The results presented above prove that the Pt NPs-doped MXene composite material was successfully synthesized.

The optical characteristics of Pt@MXene were characterized by UV–Vis absorption. The typical broad peak of MXene at approximately 270 nm was observed in the UV–Vis spectrum (Figure 1E).[37] Meanwhile, there has no obvious absorption peak in the UV–Vis region for Pt NPs, which is also compatible with the results of previous studies.[38] Doping MXene with Pt NPs resulted in a significantly higher absorbance at 355 nm (the working wavelength of the LDI MS laser) than that of MXene, which indicated that Pt@MXene can be applied for LDI MS spectrometer and have the potentials to effectively absorb laser energy and improve the desorption/ionization efficiency of samples. The absorption peak of Pt@MXene appeared at a slightly higher wavelength (290 nm) than that of MXene, may be corresponding to the coupling between Pt NPs and MXene according to previous reports.[39] These results prove that Pt@MXene has superior light-harvesting ability to MXene and can effectively absorb laser energy to promote the desorption/ionization process.

The X-ray diffraction (XRD) patterns of Pt@MXene and MXene are shown in Figure 1F. From XRD analysis results, the (002) diffraction peak of Ti_3AlC_2, MXene, and Pt@MXene exists obvious difference. The (002) diffraction peak of MXene broadened and shifted toward the lower 2 theta angle from 9.5° to 6.3° compared to the Ti_3AlC_2, which because of the removal of the Al layer from Ti_3AlC_2 resulting in a widened d-spacing of MXene sheets.[40] After the deposition of Pt NPs on MXene, the (002) peak appeared at a lower angle than in the original MXene pattern, which implies a further structural expansion of the MXene sheets.[41] The peaks at $2\theta = 39.7°$, 46.2°, 67.5°, and 81.4° correspond to the (111), (200), (220), and (311) crystal planes of Pt, respectively,[42] and are the same as those previously reported,[33] confirming that Pt@MXene was successfully prepared.

The functional groups of the Pt@MXene composite were characterized by Fourier transform infrared spectra (FT-IR). Figure 1G shows the FT-IR spectra, in which the peaks at 3369, 1620, 801, and 639 cm^{-1} were attributed to O-H, C=O, C-F, and Ti-O stretching vibrations, respectively.[29,32,43,44] Pt@MXene has basically the same functional groups as MXene, possibly because doping with Pt NPs forms a new nano hybrid without changing the surface structure of MXene.[45]

The design of the metal/MXene structure is essential for LDI MS. MXene nanosheets provide loading sites for Pt NPs because of the abundant functional groups (-O,-OH, and-F) and defects/vacancies on the surface. After a self-reduction reaction, $[PtCl_6]^{2-}$ can be reduced to Pt NPs on MXene and be firmly adsorbed to the interlayer and surface of MXene sheets by electrostatic interactions, in which MXene functioned as the reducing agent.

X-ray photoelectron spectroscopy (XPS) was performed to further confirm the elemental composition and valence state of the Pt@MXene. The survey spectra presented in Figure 1H shows the presence of F, O, Ti, and C elements in Pt@MXene. This result confirms the presence of MXene in the nanocomposite.[44] A characteristic elemental Pt peak was observed in the Pt@MXene spectrum (Figure 1H). In the high-resolution XPS spectrum of Pt 4f (Figure 1I), the binding energies of 70.8 and 74.0 eV correspond to Pt0 $4f_{7/2}$ and $4f_{5/2}$ orbitals, respectively, which demonstrate the successfully reduction of $[PtCl_6]^{2-}$ to Pt NPs. Moreover, the binding energies of 71.9 and 74.8 eV correspond to oxidized PtO_x,[46,47] which accounted for approximately half of the Pt0 in the material. The appearance of this peak was attributed to the formation of Ti-Pt and C-Pt coordination bonds and showed that Pt NPs were effectively doped *in situ* on the MXene nanosheets,[29] which was consistent with the TEM results. In addition to the peaks of the above-mentioned elements, TiO_2 $2p_{1/2}$, Ti^{3+} $2p_{1/2}$, TiO_2 $2p_{3/2}$, Ti^{3+} $2p_{3/2}$, and TiO_2 satellite peaks appeared (Figure 1J) in the Pt@MXene spectrum. The binding-energy peak of Ti^{3+} appeared at a slightly higher position in the Pt@MXene spectrum than in the MXene spectrum,[33] consistent with the previous ref. 32. It has been reported that the shifting of the binding energy of elements may be because of interactions or electron exchange between different elements.[48] Therefore, it is presumed that the binding energy shift of Ti^{3+} in Pt@MXene may be caused by the interaction or partial electron transfer between Pt and Ti.

Thus, Pt@MXene is a favorable laser energy receptor for the desorption/ionization process. Compared with some popular high-performance inorganic materials, such as titanium nanosheets,[49] non-metallic semiconductors (black phosphorus,[50,51] selenium[52]), and composite hydrogel materials,[22,53] Pt@MXene has a maximum UV absorption peak position that better matches the operational laser wavelength, richer surface functional groups, and better stability.

Pt@MXene-assisted SALDI MS analysis of various small-molecule natural products

The matrix/substrate concentration is an important factor affecting the efficacy of analyte desorption/ionization in LDI MS.[54] We first evaluated the optimal concentration of Pt@MXene using natural small molecules (phenylalanine (Phe), abscisic acid (ABA), GP, TS). Pt@MXene aqueous dispersions of seven concentrations (0.01 $mg{\cdot}mL^{-1}$, 0.1 $mg{\cdot}mL^{-1}$, 0.5 $mg{\cdot}mL^{-1}$, 1 $mg{\cdot}mL^{-1}$, 1.5 $mg{\cdot}mL^{-1}$, 2 $mg{\cdot}mL^{-1}$ and 5 $mg{\cdot}mL^{-1}$) were used for SALDI MS to detect the target ions. The highest MS signal intensity was obtained at concentrations of 1.0 $mg{\cdot}mL^{-1}$ and 1.5 $mg{\cdot}mL^{-1}$ Pt@MXene aqueous dispersion (Figure S1), and there was no significant difference ($p > 0.05$) in the signal response obtained at these two concentrations. To obtain the best detection results and save costs, 1 $mg{\cdot}mL^{-1}$ was chosen as the Pt@MXene concentration for subsequent experiments.

Next, the performance of Pt@MXene as a substrate was evaluated using natural small-molecule model analytes (amino acids and phytohormones). We performed a comparative study of the desorption/ionization

efficiency of Pt@MXene against different substrates (MXene and GO) and an organic matrix (CHCA). GO is a carbon material that is considered an effective substrate because of its good thermoelectric properties and clean background in LDI MS detection of natural small molecules (such as amino acids,[55] saccharides,[56] lipids,[57] and biogenic amines[58]). Thus, the effects of using GO and Pt@MXene as substrates in SALDI MS were compared. Clearly lower background noise interference was obtained by using Pt@MXene than by using MXene, GO, and CHCA matrix (Figure S2).

Figures 2A and 2B show that Pt@MXene exhibited superior performance to MXene, GO, and CHCA for the detection of small molecules. All 6 amino acids were detected with high intensity by using Pt@MXene, whereas MXene and GO could only detect all amino acids with relatively low intensity (Figure 2A). All 7 phytohormones were detected by using Pt@MXene (Figure 2B). However, only 6 phytohormones were detected using MXene, and only 4 phytohormones were detected using GO. The complex background interference of the organic matrices significantly reduced the detection efficiency. Only 4 amino acids and 5 phytohormones were detected using CHCA. More analyte signal peaks could be identified by using Pt@MXene than by using the other substrates and matrix, which may facilitate preliminary identification of a target (Figure 2C). The superior SALDI MS efficiency of Pt@MXene is mainly ascribed to its synergetic effect, exhibit excellent electron conductivity and efficient catalytic properties.[59,60] Strong electronic coupling between Pt NPs and MXene enhances the efficiency of separation of electrons and holes.[29,33] Under laser irradiation, the metal NPs exhibit unique localized surface plasma resonance properties.[25] Pt NPs act as an antenna to directly convert absorbed laser energy into hot carriers and promote rapid charge transfer.[61,62] Thus, the Pt@MXene offered a stronger desorption/ionization efficiency of analytes.

The applicability of Pt@MXene to the detection of different small-molecule natural products, including carbohydrates (glucose, sucrose, and maltose), organic acids (succinic acid, malic acid, and ascorbic acid), alkaloids (strychnine, matrine, and berberine), and other products (isoquercitrin, loganin, and stearic acid), by SALDI MS in positive ion mode was tested (Figures 3 and S3). As expected, Pt@MXene exhibited a higher LDI efficiency than MXene, GO, and CHCA. The highest signal intensity for all the analytes was obtained by using Pt@MXene compared to only a few low-abundance signals using MXene and GO and no alkaloid and stearic acid signals using CHCA. Overall, Pt@MXene is an effective substrate for SALDI MS analysis of small-molecule natural products because it provides relatively low background noise, high detection sensitivity, wide molecular coverage, and enhanced the desorption/ionization efficiency of analytes.

Evaluation of salt tolerance, protein tolerance, repeatability, and sensitivity of Pt@MXene

Complex biological samples often contain salt ions or protein molecules that may interfere with the desorption/ionization of the analytes. Therefore, it is essential for a substrate to have good salt and protein tolerance. The anti-interference ability of Pt@MXene to salt ions and proteins was investigated by simulating an environment with a high concentration of salt and protein. A representative analyte (ABA) was used as the analysis model for protein tolerance and repeatability tests. Figure 4A shows that for the sample with an added salt solution (0.5 M NaCl and 0.5 M KCl), high-intensity target signal peaks were still obtained by using Pt@MXene. The $[M + K]^+$ peak was significantly suppressed in the high-concentration protein solution, but a high-intensity $[M + Na]^+$ peak was clearly observed. Hence, the Pt@MXene substrate has good salt and protein tolerance that can be used to enhance LDI MS analysis of complex biological samples.

The repeatability of Pt@MXene was investigated by using standard samples of two concentrations (5 $ng \cdot \mu L^{-1}$ and 15 $ng \cdot \mu L^{-1}$) at 8 different positions on the same substrate (intraspot points) and 8 different substrates (interspot points) (Figures 4B and 4C). The results showed no significant differences in the signal-to-noise ratios (S/N) of the analytes at the intraspot and interspot points, and all the corresponding coefficients of variation (CVs) were less than 8%. This result showed that using the Pt@MXene substrate enhanced the signal reproducibility.[54] Next, the response of the Pt@MXene substrate to low concentration samples was verified. GP and TS were used as analytical models to investigate the limit of detection (LOD) (S/N = 3) and the limit of quantitation (LOQ) (S/N = 10). Analytes were deposited on the substrate and serially diluted until S/N = 3 and S/N = 10. The LOD and LOQ of GP and TS were as follows: GP LOD = 0.5 $ng \cdot \mu L^{-1}$, LOQ = 1 $ng \cdot \mu L^{-1}$; TS LOD = 0.1 $ng \cdot \mu L^{-1}$, and LOQ = 0.2 $ng \cdot \mu L^{-1}$. The proposed approach exhibits higher sensitivity than some conventional liquid chromatography.[63,64] Note that existing analytical methods with high stability and precision are usually time-consuming and require the use of large

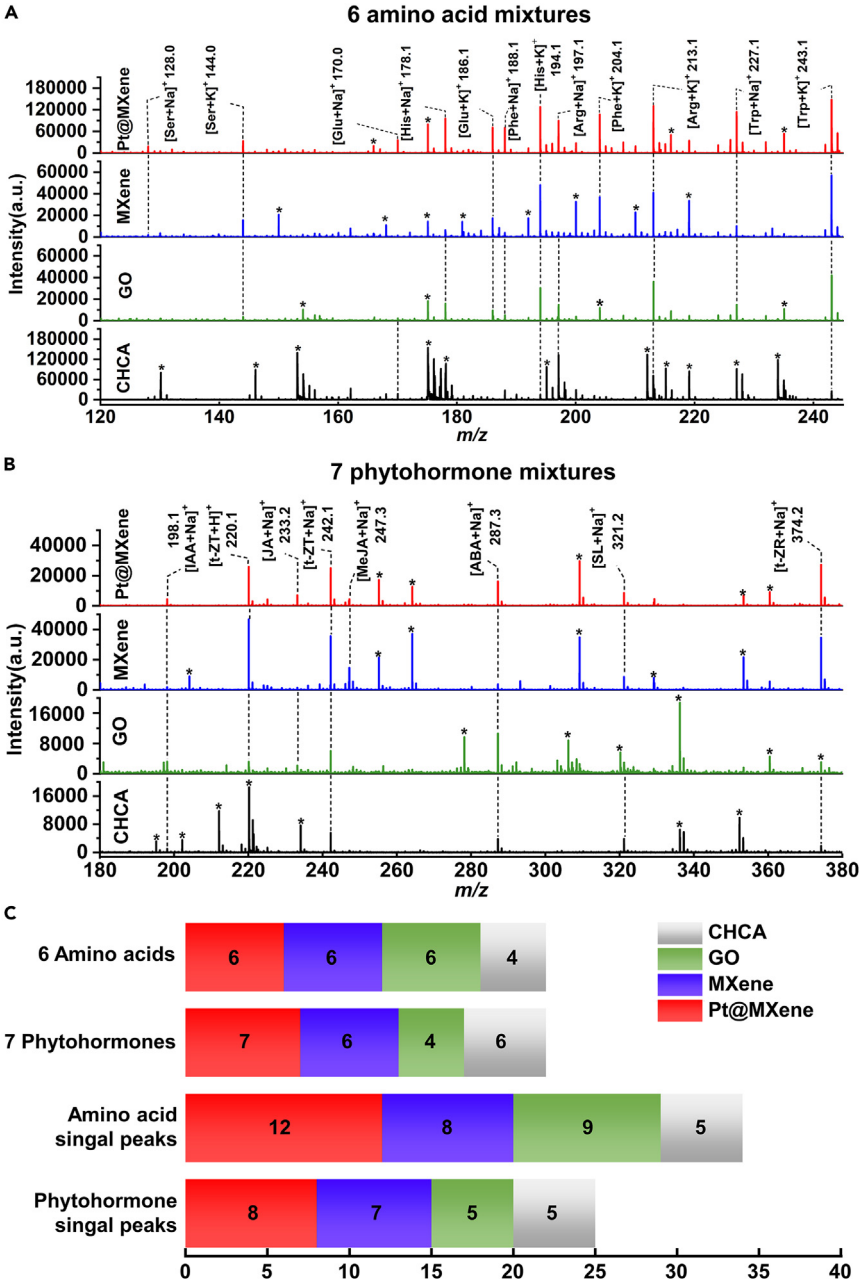

Figure 2. LDI MS analysis of amino acids and phytohormones

LDI MS spectra of (A) 6 amino acid standard mixtures, (B) 7 phytohormone standard mixtures and (C) the number of detected compounds and the signal peaks identified by using three substrates (Pt@MXene, MXene, and GO) and a CHCA matrix. *Background peak.

quantities of solvents and complex operating procedures.[5–7] By contrast, Pt@MXene-assisted LDI MS has the advantages of facile operation, the use of a low solvent volume (only 1 μL), rapid analysis (only seconds per sample), and no derivatization required.

Quantitative analysis of small-molecule natural products in *G. scabra* and *S. miltiorrhiza*

Many studies have shown that the secondary metabolites of medicinal plants are extremely valuable. GP is a major iridoid compound in Gentianaceae herbs.[65] It has been proven that GP has anti-inflammatory and gastric acid secretion-promoting biological activities.[66] In addition, Labiatae plants are widely planted

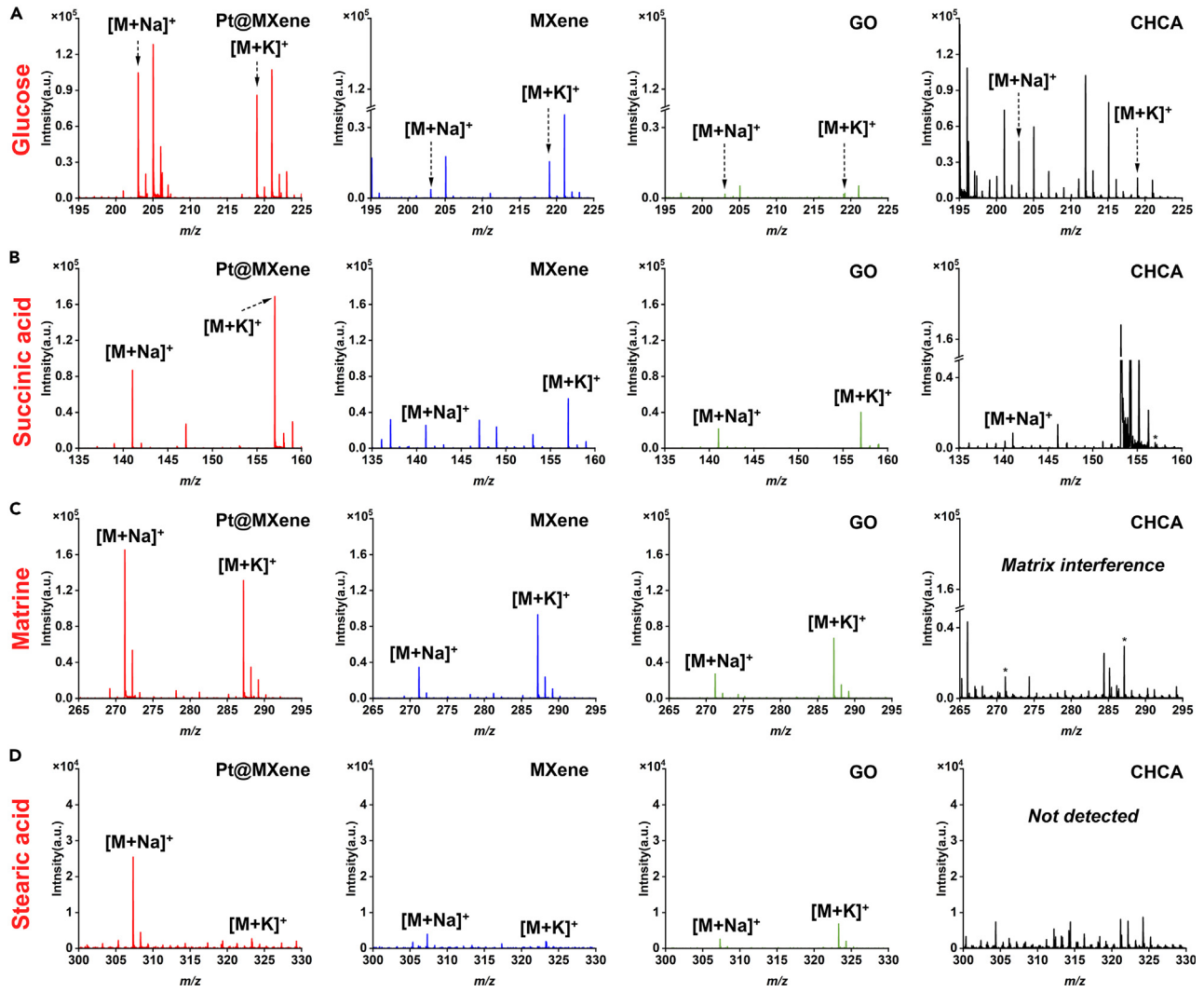

Figure 3. LDI MS analysis of various small-molecule natural products

LDI MS spectra of (A) Carbohydrate, (B) Organic acid, (C) Alkaloid and (D) other product using three substrates (Pt@MXene, MXene, and GO) and a CHCA matrix. The concentration of each analyte is 1 mg·mL^{-1} *Background peak.

worldwide. *S. miltiorrhiza* is a representative species with high medicinal value.[67] *S. miltiorrhiza* is rich in tanshinone compounds and has been used for a long period to treat blood diseases.[68] Therefore, qualitative and quantitative analyses of GP and TS in medicinal plants are necessary.

Currently, the organic matrix and sample mixture often form non-uniform crystals because of the solvent effect. This phenomenon results in uneven laser energy during analysis or ionization and desorption processes.[69] Therefore, quantification by MALDI MS is unsatisfactory. To solve these problems, an internal-standard quantitative method based on a Pt@MXene substrate was developed in this study to quantify GP in *G. scabra* and TS in *S. miltiorrhiza*. Here, vitamin A acid (VAA) was chosen as the internal standard (IS) because it has stable chemical properties and high signal peak intensity with no interferences from other analytes. Samples at different concentrations were mixed with equal volumes of VAA solution for detection. Figure S4 shows the characteristic signal peaks for GP ([M + Na]$^+$, *m/z* 379.1; [M + K]$^+$, *m/z* 395.2) and TS ([M + Na]$^+$, *m/z* 317.1; [M + K]$^+$, *m/z* 333.2) in the mass spectra. The sum of the peak areas of [M + Na]$^+$ and [M + K]$^+$ was selected for the test sample to objectively include all ionic behaviors and simulate the detection scenario of real samples. The calibration curves were linearly regressed using the ratio of the peak areas of the sample and the IS as the Y axis and the sample concentration as the X axis. In Figures 5A and 5B, the detected characteristic signal peaks of [M + Na]$^+$ and [M + K]$^+$ of selected

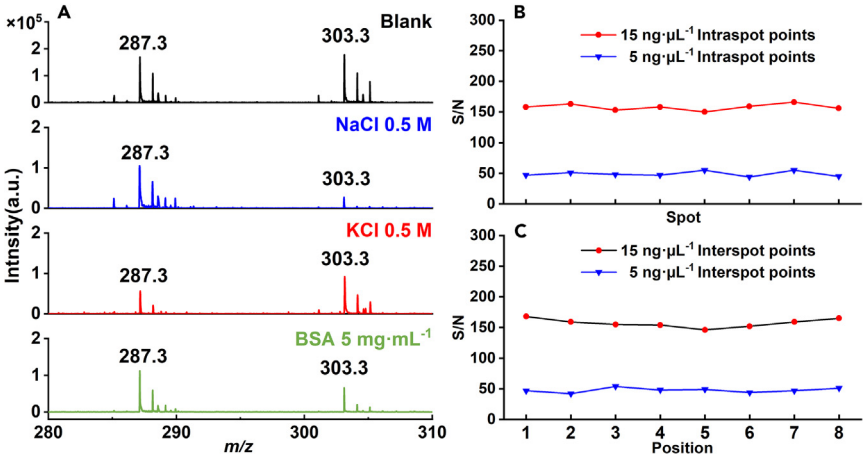

Figure 4. Evaluation of salt and protein tolerance and reproducibility of Pt@MXene as the SALDI MS substrate

(A) Mass spectra of an ABA standard (500 ng·μL^{-1}) with MeOH, NaCl (0.5 M), KCl (0.5 M), and BSA (5 mg·mL^{-1}).

(B) 8 different positions within the same target spot and the CV are 3.24% and 7.65%.

(C) 8 different target spots with different positions and the CV are 7.73% and 4.54%.

analytes are marked with asterisks, and detailed information for the MS peaks is shown in Table S1. The following standard curve was obtained using Pt@MXene: GP (R^2 = 0.9954, 25–400 ng·μL^{-1}, Y = 0.0164X+0.0852) for an IS concentration of 20 ng·μL^{-1}; TS (R^2 = 0.9956, 15–100 ng·μL^{-1}, Y = 0.257X+0.333) for an IS concentration of 30 ng·μL^{-1} (Figures 5A and 5B). The good linear relationship

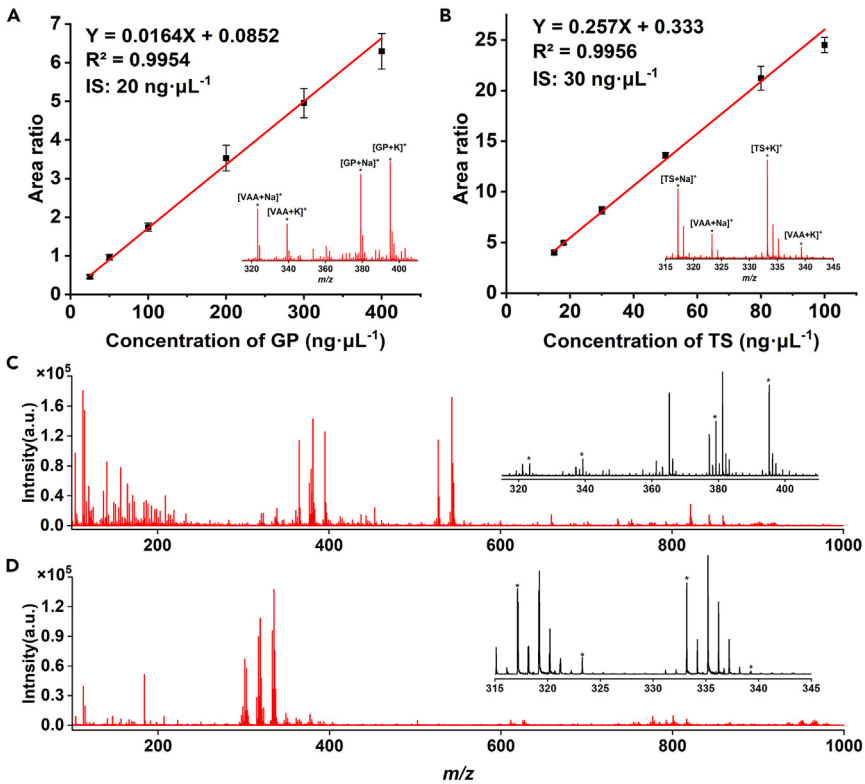

Figure 5. Quantitative analysis of natural products in real samples by SALDI MS

SALDI mass spectra and calibration curves for (A) GP in the concentration range of 25–400 ng·μL^{-1} and (B) TS in the concentration range of 15–100 ng·μL^{-1}; SALDI mass spectra for (C) *G. scabra* extract and (D) *S. miltiorrhiza* extract. The error bars were calculated as S.D. of 8 experiments. *Target peak.

Table 1. Determination of the contents of GP and TS in medicinal plants by SALDI MS and HPLC

Samples	Analyte	SALDI-MS[b] ($ng \cdot \mu L^{-1}$)	RSD[a] (%)	HPLC[b] ($ng \cdot \mu L^{-1}$)	RSD[a] (%)	Relative Error[c] (%)
G.scabra extract	GP	775.44	6.29%	773.16	1.77%	2.96%
S.miltiorrhiza extract	TS	156.08	5.66%	159.45	1.26%	2.11%

[a]The RSD was calculated from 10 replicate experiments for SALDI MS and 3 replicate experiments for HPLC.
[b]No significant difference was obtained for the substance content using the two analytical methods ($p > 0.05$).
[c]The relative error was determined using the HPLC detection results as the true value and the SALDI MS detection results as the measured value.

between the peak area ratio (of GP and TS) and the sample concentration ($R^2 > 0.99$) proved the effectiveness of this method for quantification.

Next, the practicability of the method was further assayed by analysis of the content of small-molecule natural products in two medicinal plants (*G. scabra* and *S. miltiorrhiza*). The original mass spectra of the two medicinal plants were shown in Figures 5C and 5D. The results were shown in Table 1, the content of the target compounds determined by SALDI MS was almost consistent with the HPLC detection results (Figures S7–S9). This result demonstrated that Pt@MXene platform can be used to obtain accurate quantitative (relative error <3%) information on natural products in medicinal plants. LDI-TOF/TOF MS/MS was used to confirm the structure of the target analytes (Figures S5 and S6), and information on all the MS peaks is presented in Tables S2 and S3.

Conclusion

In this study, a Pt@MXene nanocomposite was successfully prepared by a one-step reduction method. This material is an ideal SALDI MS substrate for the analysis of small-molecule natural products in positive mode.

The structural properties, elemental composition, and valence state of Pt@MXene were characterized by UV–Vis, TEM, XRD, XPS, and FT-IR. Compared with a traditional organic matrix (CHCA) and two nanosubstrates (MXene and GO), Pt@MXene exhibited the lowest background, the strongest signal peak intensity, and the widest molecular detection coverage. Moreover, Pt@MXene showed excellent salt and protein tolerance, good repeatability, and high detection sensitivity. This substrate was used in conjunction with the internal standard method to yield an accurate content of target molecules in medicinal plants, including GP in *G. scabra* and TS in *S. miltiorrhiza*. Hence, this method has high application potential for the rapid and accurate detection of small-molecule natural products and serves as a valuable reference for the design of other high-performance substrates for SALDI MS.

Limitations of this study

An efficient Pt@MXene was synthesized as a substrate for high-throughput detection and quantification of natural small molecules by SALDI MS in this study. However, more biosamples need to be evaluated to determine the applicability of this substrate to the detection of natural small molecules in different types of complex samples (such as body fluids, organs, or microbial fermentation products).

STAR★METHODS

Detailed methods are provided in the online version of this paper and include the following:

- KEY RESOURCES TABLE
- RESOURCE AVAILABILITY
  - Lead contact
  - Materials availability
  - Data and code availability
- EXPERIMENTAL MODEL AND SUBJECT DETAILS
- METHOD DETAILS
  - Chemicals and reagents
  - Synthesis of Pt@MXene
  - Material characterization
  - Sample preparation for mass spectrometry analysis

- SALDI MS detection of small-molecule natural products in medicinal plants
- HPLC quantitation of small-molecule natural products in *G. scabra* and *S. miltiorrhiz*
- Mass spectrometry data collection and processing
- Risk analysis

● QUANTIFICATION AND STATISTICAL ANALYSIS

SUPPLEMENTAL INFORMATION

Supplemental information can be found online at https://doi.org/10.1016/j.isci.2023.106622.

ACKNOWLEDGMENTS

This study was supported by China Agriculture Research System of MOF and MARA, National Natural Science Foundation of China (42007218), the Major Expenditure Increase and Reduction Projects at the Central Government (2060302), Science, Education and Industry Integration Innovation Pilot Project from Qilu University of Technology (Shandong Academy of Sciences) (2022JBZ02-04).

AUTHOR CONTRIBUTIONS

G.Z., Methodology, Formal analysis, Data curation, Investigation, Visualization, Writing – original draft. Q.H., Methodology, Formal analysis, and Supervision. H.D., L.C., and L.L., Formal analysis and Data curation. L.L., supervised and statistical analysis. Y.W., Visualization. C.M.; W.X., Conceptualization, Resources, Supervision, Funding acquisition, Writing – review and editing.

DECLARATION OF INTERESTS

The authors declare no competing interests.

Received: November 12, 2022
Revised: February 1, 2023
Accepted: March 31, 2023
Published: April 8, 2023

REFERENCES

1. Dixon, R.A. (1999). Plant natural products: the molecular genetic basis of biosynthetic diversity. Curr. Opin. Biotechnol. *10*, 192–197. https://doi.org/10.1016/S0958-1669(99)80034-2.

2. Guo, L., Yao, H., Chen, W., Wang, X., Ye, P., Xu, Z., Zhang, S., and Wu, H. (2022). Natural products of medicinal plants: biosynthesis and bioengineering in post-genomic era. Hortic. Res. *9*, uhac223. https://doi.org/10.1093/hr/uhac223.

3. Jørgensen, K., Rasmussen, A.V., Morant, M., Nielsen, A.H., Bjarnholt, N., Zagrobelny, M., Bak, S., and Møller, B.L. (2005). Metabolon formation and metabolic channeling in the biosynthesis of plant natural products. Curr. Opin. Plant Biol. *8*, 280–291. https://doi.org/10.1016/j.pbi.2005.03.014.

4. Zhao, D., Ma, C., Gao, M., Li, Y., Yang, B., Li, H., Zhang, R., Hao, M., Huang, J., Liang, K., et al. (2021). Super-assembled sandwich-like Au@MSN@Ag nanomatrices for high-throughput and efficient detection of small biomolecules. Nano Res. *15*, 2722–2733. https://doi.org/10.1007/s12274-021-3741-0.

5. Móricz, Á.M., and Ott, P.G. (2022). Separation and detection of apricot leaf triterpenes by high-performance thin-layer chromatography combined with direct bioautography and mass spectrometry. J. Chromatogr. A *1675*, 463167. https://doi.org/10.1016/j.chroma.2022.463167.

6. Xiao, H., Liu, P., Zheng, S., Wang, X., Ding, J., and Feng, Y. (2020). Screening of amino acids in dried blood spots by stable isotope derivatization-liquid chromatography-electrospray ionization mass spectrometry. Chin. Chem. Lett. *31*, 2423–2427. https://doi.org/10.1016/j.cclet.2020.03.003.

7. Soyseven, M., Sezgin, B., and Arli, G. (2022). A novel, rapid and robust HPLC-ELSD method for simultaneous determination of fructose, glucose and sucrose in various food samples: method development and validation. J. Food Compos. Anal. *107*, 104400. https://doi.org/10.1016/j.jfca.2022.104400.

8. He, H., Guo, Z., Wen, Y., Xu, S., and Liu, Z. (2019). Recent advances in nanostructure/nanomaterial-assisted laser desorption/ionization mass spectrometry of low molecular mass compounds. Anal. Chim. Acta *1090*, 1–22. https://doi.org/10.1016/j.aca.2019.08.048.

9. Tan, W., Xu, X., Lv, Y., Lei, W., Hu, K., Ye, F., and Zhao, S. (2021). Sulfonic acid functionalized hierarchical porous covalent organic frameworks as a SALDI-TOF MS matrix for effective extraction and detection of paraquat and diquat. J. Colloid Interface Sci. *603*, 172–181. https://doi.org/10.1016/j.jcis.2021.06.077.

10. Li, X., Kulkarni, A.S., Liu, X., Gao, W.Q., Huang, L., Hu, Z., and Qian, K. (2021). Metal-organic framework hybrids aid metabolic profiling for colorectal cancer. Small Methods *5*, 2001001. https://doi.org/10.1002/smtd.202001001.

11. Li, R., Zhou, Y., Liu, C., Pei, C., Shu, W., Zhang, C., Liu, L., Zhou, L., and Wan, J. (2021). Design of multi-shelled hollow Cr_2O_3 spheres for metabolic fingerprinting. Angew. Chem., Int. Ed. Engl. *60*, 12504–12512. https://doi.org/10.1002/anie.202101007.

12. Samarah, L.Z., and Vertes, A. (2020). Mass spectrometry imaging based on laser desorption ionization from inorganic and nanophotonic platforms. View *1*, 20200063. https://doi.org/10.1002/viw.20200063.

13. Guo, Z., Zhang, Q., Zou, H., Guo, B., and Ni, J. (2002). A method for the analysis of low-mass molecules by MALDI-TOF mass spectrometry. Anal. Chem. *74*, 1637–1641. https://doi.org/10.1021/ac010979m.

14. Whelan, L.C., Power, K.A.R., McDowell, D.T., Kennedy, J., and Gallagher, W.M. (2008). Applications of SELDI-MS technology in oncology. J. Cell Mol. Med. *12*, 1535–1547.

https://doi.org/10.1111/j.1582-4934.2008.00250.x.

15. Su, H., Li, X., Huang, L., Cao, J., Zhang, M., Vedarethinam, V., Di, W., Hu, Z., and Qian, K. (2021). Plasmonic alloys reveal a distinct metabolic phenotype of early gastric cancer. Adv. Mater. *33*, 2007978. https://doi.org/10.1002/adma.202007978.

16. Gan, J., Wei, X., Li, Y., Wu, J., Qian, K., and Liu, B. (2015). Designer SiO_2@Au nanoshells towards sensitive and selective detection of small molecules in laser desorption ionization mass spectrometry. Nanomedicine *11*, 1715–1723. https://doi.org/10.1016/j.nano.2015.06.010.

17. Wu, B.S., Gopal, J., Hua, P.Y., and Wu, H.F. (2016). Graphene nanosheet mediated MALDI-MS (GN-MALDI-MS) for rapid, *in situ* detection of intact incipient biofilm on material surfaces. Mater. Sci. Eng. C Mater. Biol. Appl. *66*, 285–296. https://doi.org/10.1016/j.msec.2016.04.053.

18. Law, K.P., and Larkin, J.R. (2011). Recent advances in SALDI-MS techniques and their chemical and bioanalytical applications. Anal. Bioanal. Chem. *399*, 2597–2622. https://doi.org/10.1007/s00216-010-4063-3.

19. Sagandykova, G., Pryshchepa, O., Rafińska, K., Mametov, R., Madajski, P., and Pomastowski, P. (2022). LDI-MS performance of gold nanostars as an inorganic matrix for low molecular weight analytes. Int. J. Mass Spectrom. *478*, 116872. https://doi.org/10.1016/j.ijms.2022.116872.

20. Ma, C., Wang, X., Zhang, H., Liu, W., Wang, D., Liu, F., Lu, H., and Huang, L. (2022). High-throughput screening and spatial profiling of low-mass pesticides using a novel Ti_3C_2 MXene nanowire (TMN) as MALDI MS matrix. Chemosphere *286*, 131826. https://doi.org/10.1016/j.chemosphere.2021.131826.

21. Ghidiu, M., Lukatskaya, M.R., Zhao, M.-Q., Gogotsi, Y., and Barsoum, M.W. (2014). Conductive two-dimensional titanium carbide 'clay' with high volumetric capacitance. Nature *516*, 78–81. https://doi.org/10.1038/nature13970.

22. Xing, C., Chen, S., Liang, X., Liu, Q., Qu, M., Zou, Q., Li, J., Tan, H., Liu, L., Fan, D., and Zhang, H. (2018). Two-dimensional MXene (Ti_3C_2)-integrated cellulose hydrogels: toward smart three-dimensional network nanoplatforms exhibiting light-induced swelling and bimodal photothermal/chemotherapy anticancer activity. ACS Appl. Mater. Interfaces *10*, 27631–27643. https://doi.org/10.1021/acsami.8b08314.

23. Jiang, Y., Sun, J., Cui, Y., Liu, H., Zhang, X., Jiang, Y., and Nie, Z. (2019). Ti_3C_2 MXene as a novel substrate provides rapid differentiation and quantitation of glycan isomers with LDI-MS. Chem. Commun. (J. Chem. Soc. Sect. D) *55*, 10619–10622. https://doi.org/10.1039/c9cc04467a.

24. Gao, Q., Pan, Y., Zheng, G., Liu, C., Shen, C., and Liu, X. (2021). Flexible multilayered MXene/thermoplastic polyurethane films with excellent electromagnetic interference shielding, thermal conductivity, and management performances. Adv. Compos. Hybrid Mater. *4*, 274–285. https://doi.org/10.1007/s42114-021-00221-4.

25. Hartland, G.V., Besteiro, L.V., Johns, P., and Govorov, A.O. (2017). What's so hot about electrons in metal nanoparticles? ACS Energy Lett. *2*, 1641–1653. https://doi.org/10.1021/acsenergylett.7b00333.

26. Nizioł, J., Rode, W., Zieliński, Z., and Ruman, T. (2013). Matrix-free laser desorption-ionization with silver nanoparticle-enhanced steel targets. Int. J. Mass Spectrom. *335*, 22–32. https://doi.org/10.1016/j.ijms.2012.10.009.

27. Huang, L., Gurav, D.D., Wu, S., Xu, W., Vedarethinam, V., Yang, J., Su, H., Wan, X., Fang, Y., Shen, B., et al. (2019). A multifunctional platinum nanoreactor for point-of-care metabolic analysis. Matter *1*, 1669–1680. https://doi.org/10.1016/j.matt.2019.08.014.

28. Kawasaki, H., Yonezawa, T., Watanabe, T., and Arakawa, R. (2007). Platinum nanoflowers for surface-assisted laser desorption/ionization mass spectrometry of biomolecules. J. Phys. Chem. C *111*, 16278–16283. https://doi.org/10.1021/jp075159d.

29. Min, S., Xue, Y., Wang, F., Zhang, Z., and Zhu, H. (2019). $Ti_3C_2T_x$ MXene nanosheet-confined Pt nanoparticles efficiently catalyze dye-sensitized photocatalytic hydrogen evolution reaction. Chem. Commun. (J. Chem. Soc. Sect. D) *55*, 10631–10634. https://doi.org/10.1039/c9cc05489h.

30. Zhu, Y., Wang, Z., Zhao, R., Zhou, Y., Feng, L., Gai, S., and Yang, P. (2022). Pt decorated $Ti_3C_2T_x$ MXene with NIR-II light amplified nanozyme catalytic activity for efficient phototheranostics. ACS Nano *16*, 3105–3118. https://doi.org/10.1021/acsnano.1c10732.

31. Li, Z., Xu, D., Deng, Z., Yin, J., Qian, Y., Hou, J.T., Ding, X., Shen, J., and He, X. (2023). Single-atom-catalyzed MXene-based nanoplatform with photo-enhanced peroxidase-like activity nanotherapeutics for staphylococcus aureus infection. Chem. Eng. J. *452*, 139587. https://doi.org/10.1016/j.cej.2022.139587.

32. Chen, Q., Jiang, W., and Fan, G. (2020). Pt nanoparticles on $Ti_3C_2T_x$-based MXenes as efficient catalysts for the selective hydrogenation of nitroaromatic compounds to amines. Dalton Trans. *49*, 14914–14920. https://doi.org/10.1039/d0dt02594a.

33. Rasheed, P.A., Pandey, R.P., Jabbar, K.A., and Mahmoud, K.A. (2021). Platinum nanoparticles/$Ti_3C_2T_x$ (MXene) composite for the effectual electrochemical sensing of Bisphenol A in aqueous media. J. Electroanal. Chem. *880*, 114934. https://doi.org/10.1016/j.jelechem.2020.114934.

34. Zhang, J., Zhao, Y., Guo, X., Chen, C., Dong, C.L., Liu, R.S., Han, C.P., Li, Y., Gogotsi, Y., and Wang, G. (2018). Single platinum atoms immobilized on an MXene as an efficient catalyst for the hydrogen evolution reaction. Nat. Catal. *1*, 985–992. https://doi.org/10.1038/s41929-018-0195-1.

35. Zhang, X., Shao, B., Sun, Z., Gao, Z., Qin, Y., Zhang, C., Cui, F., and Yang, X. (2020). Platinum nanoparticle-deposited $Ti_3C_2T_x$ MXene for hydrogen evolution reaction. Ind. Eng. Chem. Res. *59*, 1822–1828. https://doi.org/10.1021/acs.iecr.9b05046.

36. Zhou, R., Tu, B., Xia, D., He, H., Cai, Z., Gao, N., Chang, G., and He, Y. (2022). High-performance Pt/$Ti_3C_2T_x$ MXene based graphene electrochemical transistor for selective detection of dopamine. Anal. Chim. Acta *1201*, 339653. https://doi.org/10.1016/j.aca.2022.339653.

37. Kumar, S., Lei, Y., Alshareef, N.H., Quevedo-Lopez, M.A., and Salama, K.N. (2018). Biofunctionalized two-dimensional Ti_3C_2 MXenes for ultrasensitive detection of cancer biomarker. Biosens. Bioelectron. *121*, 243–249. https://doi.org/10.1016/j.bios.2018.08.076.

38. Mafuné, F., and Kondow, T. (2004). Selective laser fabrication of small nanoparticles and nano-networks in solution by irradiation of UV pulsed laser onto platinum nanoparticles. Chem. Phys. Lett. *383*, 343–347. https://doi.org/10.1016/j.cplett.2003.10.149.

39. Du, X., Zhang, B., Jiang, D., and Sun, J. (2020). Visible-light triggered self-breathing-like dual-photoelectrode internal-driven self-powered sensor: metal-ligand charge transfer (MLCT) induced signal-off strategy for the microcystin-LR assay. Biosens. Bioelectron. *165*, 112414. https://doi.org/10.1016/j.bios.2020.112414.

40. Cheng, H., Pan, Y., Wang, X., Liu, C., Shen, C., Schubert, D.W., Guo, Z., and Liu, X. (2022). Ni flower/MXene-melamine foam derived 3D magnetic/conductive networks for ultra-efficient microwave absorption and infrared stealth. Nano-Micro Lett. *14*, 63. https://doi.org/10.1007/s40820-022-00812-w.

41. Wang, Y., Wang, J., Han, G., Du, C., Deng, Q., Gao, Y., Yin, G., and Song, Y. (2019). Pt decorated Ti_3C_2 MXene for enhanced methanol oxidation reaction. Ceram. Int. *45*, 2411–2417. https://doi.org/10.1016/j.ceramint.2018.10.160.

42. Yen, M.Y., Teng, C.C., Hsiao, M.C., Liu, P.I., Chuang, W.P., Ma, C.C.M., Hsieh, C.K., Tsai, M.C., and Tsai, C.H. (2011). Platinum nanoparticles/graphene composite catalyst as a novel composite counter electrode for high performance dye-sensitized solar cells. J. Mater. Chem. *21*, 12880. https://doi.org/10.1039/c1jm11850a.

43. Li, L.X., Zhang, G.C., Sun, W.J., Zhang, H.Y., Wang, S.X., Wei, J.L., He, J.H., Song, K., and Lu, J.M. (2022). Construction of ultra-small Pt nanoparticles@$Ti_3C_2T_x$ MXene electrocatalyst for efficient and stable electrochemical hydrodechlorination of chloramphenicol. Chem. Eng. J. *433*, 134415. https://doi.org/10.1016/j.cej.2021.134415.

44. Boota, M., Anasori, B., Voigt, C., Zhao, M.Q., Barsoum, M.W., and Gogotsi, Y. (2016). Pseudocapacitive electrodes produced by oxidant-free polymerization of pyrrole between the layers of 2D titanium carbide (MXene). Adv. Mater. *28*, 1517–1522. https://doi.org/10.1002/adma.201504705.

45. Luo, J., Tao, X., Zhang, J., Xia, Y., Huang, H., Zhang, L., Gan, Y., Liang, C., and Zhang, W. (2016). Sn^{4+} ion decorated highly conductive Ti_3C_2 MXene: promising lithium-ion anodes with enhanced volumetric capacity and cyclic performance. ACS Nano *10*, 2491–2499. https://doi.org/10.1021/acsnano.5b07333.

46. Dutta, S., Ray, C., Sasmal, A.K., Negishi, Y., and Pal, T. (2016). Fabrication of dog-bone shaped Au NR_{core}–Pt/Pd_{shell} trimetallic nanoparticle-decorated reduced graphene oxide nanosheets for excellent electrocatalysis. J. Mater. Chem. *4*, 3765–3776. https://doi.org/10.1039/c6ta00379f.

47. Li, H., Han, X., Zuo, K., Li, L., Liu, J., Yuan, X., Shen, Y., Shao, M., Pang, D., Chu, Y., and Zhao, B. (2018). Ultrathin Pt_xSn_{1-x} nanowires for methanol and ethanol oxidation reactions: tuning performance by varying chemical composition. ACS Appl. Nano Mater. *50*, 1104–1115. https://doi.org/10.1021/acsanm.7b00289.

48. Greiner, M.T., Jones, T.E., Beeg, S., Zwiener, L., Scherzer, M., Girgsdies, F., Piccinin, S., Armbrüster, M., Knop-Gericke, A., and Schlögl, R. (2018). Free-atom-like *d* states in single-atom alloy catalysts. Nat. Chem. *10*, 1008–1015. https://doi.org/10.1038/s41557-018-0125-5.

49. Xie, Z., Chen, S., Duo, Y., Zhu, Y., Fan, T., Zou, Q., Qu, M., Lin, Z., Zhao, J., Li, Y., et al. (2019). Biocompatible two-dimensional titanium nanosheets for multimodal imaging-guided cancer theranostics. ACS Appl. Mater. Interfaces *11*, 22129–22140. https://doi.org/10.1021/acsami.9b04628.

50. Xie, Z., Peng, M., Lu, R., Meng, X., Liang, W., Li, Z., Qiu, M., Zhang, B., Nie, G., Xie, N., et al. (2020). Black phosphorus-based photothermal therapy with aCD47-mediated immune checkpoint blockade for enhanced cancer immunotherapy. Light Sci. Appl. *9*, 161. https://doi.org/10.1038/s41377-020-00388-3.

51. Yin, F., Hu, K., Chen, S., Wang, D., Zhang, J., Xie, M., Yang, D., Qiu, M., Zhang, H., and Li, Z.G. (2017). Black phosphorus quantum dot based novel siRNA delivery systems in human pluripotent teratoma PA-1 cells. J. Mater. Chem. B *5*, 5433–5440. https://doi.org/10.1039/c7tb01068k.

52. Chen, S., Xing, C., Huang, D., Zhou, C., Ding, B., Guo, Z., Peng, Z., Wang, D., Zhu, X., Liu, S., et al. (2020). Eradication of tumor growth by delivering novel photothermal selenium-coated tellurium nanoheterojunctions. Sci. Adv. *6*, eaay6825. https://doi.org/10.1126/sciadv.aay6825.

53. Xing, C., Chen, S., Qiu, M., Liang, X., Liu, Q., Zou, Q., Li, Z., Xie, Z., Wang, D., Dong, B., et al. (2018). Conceptually novel black phosphorus/cellulose hydrogels as promising photothermal agents for effective cancer therapy. Adv. Healthc. Mater. *7*, 1701510. https://doi.org/10.1002/adhm.201701510.

54. Li, L., Qiu, Z., Qi, Y., Zhao, D., Ali, I., Sun, C., Xu, L., Zheng, Z., and Ma, C. (2022). AuNPs/NiFe-LDHs-assisted laser desorption/ionization mass spectrometry for efficient analysis of metronidazole and its metabolites in water samples. J. Hazard Mater. *423*, 126893. https://doi.org/10.1016/j.jhazmat.2021.126893.

55. Hong, Y.L., Seo, T.H., Jang, H., and Kim, Y.K. (2019). The effect of oxidative debris on the laser desorption/ionization efficiency of graphene oxide derivatives for mass spectrometric analysis of small molecules and synthetic polymers. Anal. Sci. *35*, 1097–1102. https://doi.org/10.2116/analsci.19P205.

56. Kim, Y.K., and Min, D.H. (2014). Mechanistic study of laser desorption/ionization of small molecules on graphene oxide multilayer films. Langmuir *30*, 12675–12683. https://doi.org/10.1021/la5027653.

57. Liang, K., Gao, H., Gu, Y., Yang, S., Zhang, J., Li, J., Wang, Y., Wang, Y., and Li, Y. (2018). Graphene oxide aggregate-assisted LDI-MS for the direct analysis of triacylglycerol in complex biological samples. Anal. Chim. Acta *1035*, 108–118. https://doi.org/10.1016/j.aca.2018.07.049.

58. Siripongpreda, T., Siralertmukul, K., and Rodthongkum, N. (2020). Colorimetric sensor and LDI-MS detection of biogenic amines in food spoilage based on porous PLA and graphene oxide. Food Chem. *329*, 127165. https://doi.org/10.1016/j.foodchem.2020.127165.

59. Cui, C., Cheng, R., Zhang, C., and Wang, X. (2020). Pt immobilized spontaneously on porous MXene/MAX hybrid monolith for hydrogen evolution reaction. Chin. Chem. Lett. *31*, 988–991. https://doi.org/10.1016/j.cclet.2019.08.026.

60. Jiang, H., Hu, Z., Gan, C., Sun, B., Kong, S., and Bian, F. (2021). Visible-light induced one-pot hydrogenation and amidation of nitroaromatics with carboxylic acids over 2D MXene-derived Pt/N-TiO_2/Ti_3C_2. Mol. Catal. *504*, 111490. https://doi.org/10.1016/j.mcat.2021.111490.

61. Clavero, C. (2014). Plasmon-induced hot-electron generation at nanoparticle/metal-oxide interfaces for photovoltaic and photocatalytic devices. Nat. Photonics *8*, 95–103. https://doi.org/10.1038/nphoton.2013.238.

62. Wei, X., Liu, Z., Jin, X., Huang, L., Gurav, D.D., Sun, X., Liu, B., Ye, J., and Qian, K. (2017). Plasmonic nanoshells enhanced laser desorption/ionization mass spectrometry for detection of serum metabolites. Anal. Chim. Acta *950*, 147–155. https://doi.org/10.1016/j.aca.2016.11.017.

63. Singh, M., Mohan, R., Mishra, S., Goyal, N., Shanker, K., Gupta, N., and Kumar, B. (2019). Ultra performance liquid chromatography coupled with principal component and cluster analysis of *Swertia chirayita* for adulteration check. J. Pharm. Biomed. Anal. *164*, 302–308. https://doi.org/10.1016/j.jpba.2018.10.054.

64. Wang, Z., Cao, B., Yu, A., Zhang, H., and Qiu, F. (2015). Ultrasound-assisted ionic liquid-based homogeneous liquid-liquid microextraction high-performance liquid chromatography for determination of tanshinones in *Salvia miltiorrhiza* Bge. root. J. Pharm. Biomed. Anal. *104*, 97–104. https://doi.org/10.1016/j.jpba.2014.11.034.

65. Sadia, S., Tariq, A., Shaheen, S., Malik, K., khan, F., Ahmad, M., Qureshi, H., and Nayyar, B.G. (2018). Ethnopharmacological profile of anti-arthritic plants of Asia-a systematic review. J. Herb. Med. *13*, 8–25. https://doi.org/10.1016/j.hermed.2018.08.003.

66. Ruan, M., Yu, B., Xu, L., Zhang, L., Long, J., and Shen, X. (2015). Attenuation of stress-induced gastrointestinal motility disorder by gentiopicroside, from *Gentiana macrophylla Pall*. Fitoterapia *103*, 265–276. https://doi.org/10.1016/j.fitote.2015.04.015.

67. Xu, H., Song, J., Luo, H., Zhang, Y., Li, Q., Zhu, Y., Xu, J., Li, Y., Song, C., Wang, B., et al. (2016). Analysis of the genome sequence of the medicinal plant *Salvia miltiorrhiza*. Mol. Plant *9*, 949–952. https://doi.org/10.1016/j.molp.2016.03.010.

68. Jassbi, A.R., Zare, S., Firuzi, O., and Xiao, J. (2015). Bioactive phytochemicals from shoots and roots of Salvia species. Phytochemistry Rev. *15*, 829–867. https://doi.org/10.1007/s11101-015-9427-z.

69. He, H., Qin, L., Zhang, Y., Han, M., Li, J., Liu, Y., Qiu, K., Dai, X., Li, Y., Zeng, M., et al. (2019). 3,4-Dimethoxycinnamic acid as a novel matrix for enhanced in situ detection and imaging of low-molecular-weight compounds in biological tissues by MALDI-MSI. Anal. Chem. *91*, 2634–2643. https://doi.org/10.1021/acs.analchem.8b03522.

70. Lorencova, L., Bertok, T., Filip, J., Jerigova, M., Velic, D., Kasak, P., Mahmoud, K.A., and Tkac, J. (2018). Highly stable $Ti_3C_2T_x$ (MXene)/Pt nanoparticles-modified glassy carbon electrode for H_2O_2 and small molecules sensing applications. Sensor. Actuat. B-Chem *263*, 360–368. https://doi.org/10.1016/j.snb.2018.02.124.

71. Balijagić, J., Janković, T., Zdunić, G., Bosković, J., Šavikin, K., Goćevac, D., Stanojković, T., Jovancević, M., and Menković, N. (2012). Chemical profile, radical scavenging and cytotoxic activity of yellow gentian leaves (*Genitaneae Luteae Folium*) grown in northern regions of Montenegro. Nat. Prod. Commun. *7*, 1487–1490. https://doi.org/10.1177/1934578X1200701119.

72. Wang, J., Zhai, W., Yu, J., Wang, J., and Dai, J. (2018). Preparation and quality evaluation of salvianolic acids and tanshinones dry powder inhalation. J. Pharmaceut. Sci. *107*, 2451–2456. https://doi.org/10.1016/j.xphs.2018.05.018.

STAR★METHODS

KEY RESOURCES TABLE

REAGENT or RESOURCE	SOURCE	IDENTIFIER
Chemicals, peptides, and recombinant proteins		
$H_2PtCl_6 \cdot 6H_2O$	Sigma Aldrich	Cat#206083; CAS: 18497-13-7
Ti_3AlC_2	Beike 2D Materials Co., Ltd	Cat#BK2020061705; CAS: 196506-01-1
Ti_3C_2	Beike 2D Materials Co., Ltd	Cat#BKC3000061
Pt nanoparticles	Hangzhou Nano-Mall Technology	Cat#FM-Pt-01
Graphene oxide	Beike 2D Materials Co., Ltd	Cat#BKJCGO
α-Cyano-4-hydroxycinnamic acid	Sigma Aldrich	Cat#C8982; CAS: 28166-41-8
Serine	National Institutes for Food and Drug Control	Cat#140688; CAS: 56-45-1
Glutamic acid	National Institutes for Food and Drug Control	Cat#140690; CAS: 56-86-0
Histidine	National Institutes for Food and Drug Control	Cat#140855; CAS: 71-00-1
Phenylalanine	National Institutes for Food and Drug Control	Cat#140676; CAS: 63-91-2
Arginine	National Institutes for Food and Drug Control	Cat#140685; CAS: 74-79-3
Tryptophan	National Institutes for Food and Drug Control	Cat#140686; CAS: 73-22-3
3-Indoleacetic acid	Shanghai Yuanye Bio-Technology Co., Ltd.	Cat#B21810; CAS: 87-51-4
Trans-zeatin	Shanghai Yuanye Bio-Technology Co., Ltd.	Cat#B25447; CAS: 1637-39-4
Jasmonic acid	Shanghai Yuanye Bio-Technology Co., Ltd.	Cat#T70282; CAS: 3572-66-5
Methyl jasmonate	Shanghai Yuanye Bio-Technology Co., Ltd.	Cat#S30685; CAS: 39924-52-2
Abscisic acid	Shanghai Yuanye Bio-Technology Co., Ltd.	Cat#B50721; CAS: 21293-29-8
Strigolactone	Shanghai Yuanye Bio-Technology Co., Ltd.	Cat#S31363; CAS: 76974-79-3
Trans-zeatin-riboside	Shanghai Yuanye Bio-Technology Co., Ltd.	Cat#B26967; CAS: 6025-53-2
Vitamin A acid	Shanghai Yuanye Bio-Technology Co., Ltd.	Cat#B21287; CAS: 302-79-4
Gentiopicroside	Chengdu DeSiTe Biological Technology Co. Ltd.	Cat#DL0070; CAS: 20831-76-9
Tanshinone IIA	Chengdu DeSiTe Biological Technology Co. Ltd.	Cat#DD0011; CAS: 568-72-9
Glucose	Chengdu DeSiTe Biological Technology Co. Ltd.	Cat#DW0005; CAS: 50-99-7
Sucrose	Chengdu DeSiTe Biological Technology Co. Ltd.	Cat#DZ0038; CAS: 57-50-1
Maltose	Chengdu DeSiTe Biological Technology Co. Ltd.	Cat#DM0046; CAS: 6363-53-7
Succinic acid	Chengdu DeSiTe Biological Technology Co. Ltd.	Cat#DH0020; CAS:110-15-6
Malic acid	Chengdu DeSiTe Biological Technology Co. Ltd.	Cat#DP0018; CAS: 6915-15-7
Ascorbic acid	Chengdu DeSiTe Biological Technology Co. Ltd.	Cat#DW0045; CAS: 50-81-7
Strychnine	Chengdu DeSiTe Biological Technology Co. Ltd.	Cat#DS0026; CAS: 57-24-9
Matrine	Chengdu DeSiTe Biological Technology Co. Ltd.	Cat#DK0009; CAS: 519-02-8
Berberine	Chengdu DeSiTe Biological Technology Co. Ltd.	Cat#DX0009; CAS: 2086-83-1

(*Continued on next page*)

Continued

REAGENT or RESOURCE	SOURCE	IDENTIFIER
Isoquercitrin	Chengdu DeSiTe Biological Technology Co. Ltd.	Cat#DY0006; CAS: 482-35-9
Loganin	Chengdu DeSiTe Biological Technology Co. Ltd.	Cat#DM0038; CAS:1852-94-2
Stearic acid	Chengdu DeSiTe Biological Technology Co. Ltd.	Cat#DY0221; CAS: 57-11-4
Software and algorithms		
Flexanalysis v4.0	Bruker Daltonics	https://www.bruker.com/zh/products-and-solutions/mass-spectrometry.html
Statistical Product Service Solutions (SPSS) v21.0	International Business Machines Corporation (IBM)	https://www.ibm.com/cn-zh/spss
Other		
rapifleX MALDI Tissuetyper™ TOF/TOF MS	Bruker Daltonics	https://www.bruker.com/zh/products-and-solutions/mass-spectrometry/maldi-tof/rapiflex-maldi-tissuetyper.html
Waters e2695 HPLC	Waters Corporation	https://www.waters.com/nextgen/cn/zh.html
SHIMADZU UV-2700 UV–VIS Spectrophotometer	SHIMADZU Corporation	https://www.shimadzu.com.cn/an/index.html
Bruker D8 Advance XRD	Bruker Daltonik GmbH	https://www.bruker.com/zh/products-and-solutions/diffractometers-and-scattering-systems/x-ray-diffractometers.html
Bruker VERTEX 70v FT-IR	Bruker Daltonik GmbH	https://www.bruker.com/zh/products-and-solutions/infrared-and-raman/ft-ir-research-spectrometers/vertex-research-ft-ir-spectrometer.html
Thermo Scientific ESCALAB Xi+ XPS	Thermo Fisher Scientific	https://www.thermofisher.cn/search/browse/category/cn/zh/90207161
Thermo Scientific Talos™ F200s TEM	Thermo Fisher Scientific	https://www.thermofisher.cn/cn/zh/home/electron-microscopy/products/transmission-electron-microscopes.html
Gentiana scabra Bge.	a pharmacy in China (Jinan, Shandong province)	Cat#JN-SYPM-20220427001
Salvia miltiorrhiza Bge.	the planting base of medicinal plants in China (Laiwu, Shandong province).	N/A

RESOURCE AVAILABILITY

Lead contact

Further information and requests for resources and reagents should be directed to and will be fulfilled by the lead contact, Chunxia Ma (machunxia8927@163.com).

Materials availability

This study did not generate new unique reagents.

Data and code availability

- Data reported in this paper will be shared by the lead contact upon request.
- This paper does not report original code.
- Any additional datasupporting findings on this study are available from the lead contact upon request.

EXPERIMENTAL MODEL AND SUBJECT DETAILS

This study does not involve animal and cellular experiments.

METHOD DETAILS

Chemicals and reagents

$H_2PtCl_6 \cdot 6H_2O$ and CHCA (≥99%) were purchased from Sigma Aldrich (St. Louis, MO, USA). Pt nanoparticle was obtained from Hangzhou Nano-Mall Technology. Serine (Ser), glutamic acid (Glu), histidine (His), phenylalanine (Phe), arginine (Arg), and tryptophan (Trp) were purchased from the National Institutes for Food and Drug Control (Beijing, China). 3-Indoleacetic acid (IAA), trans-zeatin (t-ZT), jasmonic acid (JA), methyl jasmonate (MeJA), abscisic acid (ABA), strigolactone (SL), trans-zeatin-riboside (t-ZR) and vitamin A acid (VAA) were purchased from Shanghai Yuanye Bio-Technology Co., Ltd. (Shanghai, China). All other standard samples were HPLC grade and purchased from Chengdu DeSiTe Biological Technology Co. Ltd. (Chengdu, China). Single/few-layer MXene powders and graphene oxide (GO) were obtained from Beike 2D Materials Co., Ltd. (Jiangsu, China). Chromatographic grade methanol (MeOH), acetonitrile (ACN), ethanol absolute (EtOH), and trifluoroacetic acid (TFA) were purchased from Merck (Darmstadt, Germany). Deionized water was obtained from a Milli-Q ultrapure water system in the laboratory (Millipore Corporation, Bedford, MA, USA). *G. scabra* was obtained from a pharmacy in China (Batch No: JN-SYPM-20220427001, Jinan, Shandong). *S. miltiorrhiz* was obtained from the planting base of medicinal plants in China (Laiwu, Shandong).

Synthesis of Pt@MXene

Single/few-layer MXene was prepared according to our previously reported method.[20] Firstly, 0.67 g of LiF powder was mixed with HCl (6 moL·mL^{-1}, 10 mL), and 0.1 g of Ti_3AlC_2 power was slowly added to the above solution. The obtained mixture was stirred continuously at room temperature for 24 h. The reaction produce was washed by multiple centrifugation (3500 rpm, 5 min) until the solution pH > 6. To obtain single/few-layer MXene, the precipitate was dispersed in 100 mL of deionized water and then ultrasonicated (500 W) for 3 h in argon atmosphere. Finally, the supernatant was collected by centrifugation (3500 rpm) for 1 h, followed by freeze-drying.

Pt@MXene was synthesized by a one-step reduction method according to previous reports.[47,70] In this study, MXene promoted the spontaneous reduction of $H_2PtCl_6 \cdot 6H_2O$ to Pt NPs. Finally, Pt nanoparticles were anchored on the surface of MXene nanosheets. Specifically, 10 mg of single/few-layer MXene powder were added to 20 mL of deionized water, and the sample solution was then ultrasonicated at 400 W for 20 min. Subsequently, a $H_2PtCl_6 \cdot 6H_2O$ (1 mg·mL^{-1}, 1.33 mL) solution was slowly added to the MXene solution under continuous stirring. The entire reaction was carried out for 6 hours in the dark. After the reduction reaction was completed, the resulting reaction mixtures were collected by centrifugation (9000 rpm, 5 min) and purified by washing with water three times. Finally, the composite Pt@MXene powder was obtained by the freeze-drying method. The proportion of platinum in the Pt@MXene composite was determined to be 5% by a weight calculation.

Material characterization

UV–Vis absorption spectra of Pt@MXene and MXene at the same concentration were recorded by a UV-2700 (Shimadzu, Japan) absorption spectrophotometer. Data were collected in the visible region between 200∼800 nm.

Sample solutions (5 mg·mL^{-1}, 1 mL) were prepared for X-ray diffraction (XRD) analysis by deposition on a 25 mm×25 mm transparent glass plate followed by drying. The crystal structures of the samples were determined using a D8 Advance (Bruker Daltonik GmbH, Germany) in the 2θ range of 5°∼90° (scanning speed 4°·min^{-1}).

Fourier transform infrared spectra (FT-IR) were obtained using a Vertex 70v (Bruker Daltonik GmbH, Germany), and the sample was prepared according to a reported KBr method.[45] Briefly, Pt@MXene (2 mg) and KBr (300 mg) powders were homogeneously mixed, ground well and placed in a tablet press to prepare samples for analysis.

X-ray photoelectron spectroscopy (XPS) was performed by using a ESCALAB Xi$^+$ (Thermo Fisher Scientific, USA) with a mono Alka X-ray source at a voltage of 1486.6 eV. The sample solution (5 mg·mL^{-1}) was dropped on the surface of a silicon wafer for subsequent analysis. 10 μL of the Pt@MXene or MXene solution were dropped onto a square silicon chip with dimensions of 5 mm × 5 mm and dried in a vacuum at room temperature. The aforementioned operation was repeated in triplicate. The obtained data were analyzed using Thermo Avantage v5.976 software (Thermo Fisher Scientific, USA), and the binding energies were calibrated using the C 1s peak at 284.8 eV corresponding to graphitic carbon.

Transmission electron microscopy (TEM), high-angle annular dark field-scanning transmission electron microscopy (HAADF-STEM), and energy-dispersive X-ray spectroscopy (EDS) mapping were performed using a Talos™ F200s instrument (Thermo Fisher Scientific, USA). The Pt@MXene powder was dispersed in EtOH and dropped onto a carbon-coated Cu grid, followed by drying at room temperature for 12 h.

Sample preparation for mass spectrometry analysis

Solutions of six amino acids (Ser, Glu, His, Phe, Arg, and Trp) were prepared in deionized water at a concentration of 100 ng·μL^{-1}. Solutions of seven phytohormones (IAA, t-ZT, JA, MeJA, ABA, SL, and t-ZR) were prepared in MeOH at a concentration of 100 ng·μL^{-1}. The following analytes were dissolved in appropriate solvents to produce 1 mg·mL^{-1} solutions: organic acids (succinic acid and malic acid, dissolved in MeOH and ascorbic acid, dissolved in pure water), saccharides (glucose, maltose, and sucrose, dissolved in pure water), alkaloids (matrine, berberine, and strychnine, dissolved in MeOH), and other analytes (loganin, isoquercitrin, and stearic acid, dissolved in MeOH).

GP (1 mg·mL^{-1}), TS (1 mg·mL^{-1}), and VAA (40 and 60 ng·μL^{-1}) standard solutions were prepared in MeOH. A 1 mg·mL^{-1}ABA standard was prepared in MeOH/water (1:1, *v/v*) and mixed with an equal volume of a salt solution (NaCl and KCl, 1 M) or protein (BSA, 10 mg·mL^{-1}) to investigate the detection efficiency for complex samples.

Pt@MXene powder was dispersed in deionized water at a concentration of 5 mg·mL^{-1}. The 1 mg·mL^{-1} graphene oxide (GO) and MXene dispersion were prepared in deionized water, respectively. CHCA was prepared at a concentration of 1 mg·mL^{-1} in 0.1% TFA buffer (ACN/water, 70:30, *v/v*). The ionization efficiencies of different nanomaterials and organic matrices were compared based on the signal intensity of the target peaks.

SALDI MS detection of small-molecule natural products in medicinal plants

In this experiment, natural products from two medicinal plants, *G. scabra* and *S. miltiorrhiza*, were extracted using ultrasonic-assisted extraction. In brief, 1 g of the crude powder of each medicinal material and 10 mL of EtOH were mixed in a conical flask and left at room temperature for 1 hour. Next, the mixture was ultrasonicated at 15 °C for 1 h. The output power of the ultrasonic machine was set at 300 W. The extracts were filtered through a 0.22-μm membrane before analysis.

The internal standard (IS) method was used for the quantitative analysis of the metabolites. The internal standard solution (40 ng·μL^{-1} and 60 ng·μL^{-1} VAA (IS)) was added to the extracts of *G. scabra* and *S. miltiorrhiza* in a 1:1 volume ratio, respectively. Finally, a standard curve was generated by plotting the ratio of the sum of the peak areas of the target to that of the IS as the ordinate and the target concentration as the abscissa. The final experimental result was taken as the average measurement of 10 repeated tests.

HPLC quantitation of small-molecule natural products in *G. scabra* and *S. miltiorrhiz*

The external standard method was used to quantify single compounds (GP and TS) in *G. scabra* and *S. miltiorrhiza*. A Waters e2695 HPLC instrument with a diode array detector (DAD) and reverse-phase Symmetry C-18 (Waters) column (250 mm × 4.6 mm i.d., 5 μm) was used at 25 °C. Gradient elution was employed using solution A (0.1% formic acid in water) and solution B (ACN) as mobile phases. The LC gradient elution conditions were referred to and improved from previously reported.[71,72] Among them, the HPLC analysis conditions of GP were as follows: 0∼1 min, 90%∼85% A; 1∼10 min, 85%∼70% A; 10∼15 min, 70%∼90% A; and 15.5∼20 min, 90% A, at a flow rate of 1 mL·min^{-1}. The UV−Vis wavelength of the detector was set at 270 nm, and the sample injection volume was 3 μL; TS was analyzed according to the following procedure: 0∼6 min, 39% A; 6∼20 min, 39%∼10% A; 20∼25 min, 10% A; 25∼25.5 min, 10%∼39% A; and 25.5∼30 min, 39% A, at a flow rate of 1 mL·min^{-1}. Detection was performed at a maximum absorption

wavelength of 270 nm, and the sample injection volume was 3 μL. Two analyte standard solutions were determined under the above mentioned chromatographic conditions. A quantitative linear relationship was established between the standard concentration and peak area for GP and TS. The extracts of the medicinal materials were determined under the same chromatographic conditions. The actual content of the metabolites in the samples was calculated from the average peak area and regression equation.

Mass spectrometry data collection and processing

Mass spectrometry was performed on a rapifleX MALDI Tissuetyper™ TOF/TOF MS (Bruker Daltonics, Billerica, MA) equipped with a 355-nm SmartBeam II laser. The original spectrum was obtained in positive reflection mode, the molecular weight detection range was 100∼1000 Da, and the global attenuator shift was adjusted to 15%. The mass spectra were superimposed by 200 laser shots at a frequency of 5000 Hz. The laser energy was adjusted to 45%∼60%. MALDI LIFT-TOF/TOF MS/MS operated at a pulsed voltage of 2.65 kV was used for *in situ* tandem MS/MS analysis.

For LDI MS detection, 1 μL of the nanomaterial was deposited onto a stainless-steel sample target plate, and the solvent was dried in a vacuum at 25 °C. Next, 1 μL of the sample solution was placed on the dried substrate on the target plate. Samples in the CHCA matrix were prepared using the reverse order presented above, that is, the sample was first dropped on the substrate and then covered.

The original mass spectrogram was imported into Flexanalysis version 4.0 (Build 9) software (Bruker Daltonics) for peak screening and baseline calibration.

Risk analysis

Substrates are synthesized in a well-controlled environment and no harmful chemicals are used throughout the process. All synthesis processes were carried out in controlled acid-resistant fume hoods. Vacuum drying was performed for 5∼20 minutes after the substrate was deposited on the steel target to prevent impurities from entering the mass spectrometer. The proper use of all instrumentation ensures that experimenter is not at risk.

QUANTIFICATION AND STATISTICAL ANALYSIS

The data were statistically analyzed, including determining the standard deviation (S.D.), one-way analysis of variance (ANOVA), and performing the *t* test, Duncan's test, and Tukey's test using SPSS (Version 21.0 Armonk, NY, USA). $p < 0.05$ was considered statistically significant.